SFB/CPP-14-124, DESY-15-059, CP3-Origins-2015-013 DNRF90, DIAS-2015-13

A Lattice Calculation of Parton Distributions

Constantia Alexandrou[a,b], Krzysztof Cichy[c,d], Vincent Drach[e], Elena Garcia-Ramos[c,f], Kyriakos Hadjiyiannakou[a], Karl Jansen[c], Fernanda Steffens[c], and Christian Wiese[c]

[a]Department of Physics, University of Cyprus, P.O. Box 20537, 1678 Nicosia, Cyprus
[b]The Cyprus Institute, 20 Kavafi Str., Nicosia 2121, Cyprus
[c]John von Neumann Institute for Computing (NIC), DESY, Platanenallee 6, 15738 Zeuthen, Germany
[d]Faculty of Physics, Adam Mickiewicz University, Umultowska 85, 61-614 Poznań, Poland
[e]CP^3-Origins & the DIAS, University of Southern Denmark, Campusvej 55, 5230 Odense M, Denmark
[f]Humboldt-Universität zu Berlin, Institut für Physik, Newtonstr. 15, 12489 Berlin, Germany

arXiv:1504.07455v1 [hep-lat] 28 Apr 2015

Abstract

We report on our exploratory study for the direct evaluation of the parton distribution functions from lattice QCD, based on a recently proposed new approach. We present encouraging results using $N_f = 2 + 1 + 1$ twisted mass fermions with a pion mass of about 370 MeV. The focus of this work is a detailed description of the computation, including the lattice calculation, the matching to an infinite momentum and the nucleon mass correction. In addition, we test the effect of gauge link smearing in the operator to estimate the influence of the Wilson line renormalization, which is yet to be done.

1 Introduction

Parton distribution functions (PDFs) describe the structure of hadrons by providing information on the momentum, angular momentum and spin of quarks and gluons in a hadron. Ideally, PDFs would be directly predicted by quantum chromodynamics (QCD). Confronted with results from deep inelastic scattering experiments, this would lead to a most stringent test of QCD and a deep theoretical understanding of the interaction between quarks and gluons. Naturally, lattice QCD methods, which can cover a broad energy range from the perturbative to the non-perturbative regimes, would be most suitable to compute the PDFs. However, such a calculation requires light-cone dynamics and going to short, or even zero distance on the Euclidean space-time lattice is not possible.

Nevertheless, through the operator product expansion, moments of the PDFs can be expressed in terms of matrix elements of local operators, which are accessible to lattice QCD calculations. In fact, lattice QCD calculations of the PDF's moments have been very successfully carried out with results emerging now directly at the physical value of the pion mass, see the recent reviews of Refs. [1, 2, 3, 4].

Despite the enormous activity of computing such moments in lattice QCD, it would still be highly desirable to have information on the PDFs themselves. A reconstruction of the PDFs from their moments seems unfeasible on the lattice, since higher moments show a very bad signal-to-noise ratio and are very hard to compute. A solution to this problem might be the proposal in Ref. [5], which suggests that by computing a parton quasi-distribution function, a quantity accessible to lattice computations, contact to the required physical PDFs can be established through a matching procedure. Such a matching has already been worked out in 1-loop perturbation theory [6] and a first test of the approach has been carried out in Ref. [7] using staggered fermions.

Here, we will use a different quark discretization on the lattice, namely twisted mass fermions at maximal twist [8], to conduct an exploratory study of the proposal in Ref. [5]. This lattice formulation of QCD has the advantage that all physical quantities scale with a rate of $O(a^2)$ towards the continuum limit and avoids the operator improvement necessary in other lattice QCD formulations, easing thus considerably the computations. Twisted mass lattice QCD calculations for baryons have already been carried out successfully for the baryon spectrum [9, 10, 11], for form factors and moments of PDFs [12, 13, 14, 15, 16] and also for disconnected contributions to nucleon observables [17, 18, 19].

As stated above, our work here focuses on exploring the potential of the approach in Ref. [5]. To this end, we concentrate on one ensemble of maximally twisted mass fermions at a lattice spacing of about 0.08 fm and a pion mass of about 370 MeV.

In our calculations, we obtain results for a boosting nucleon frame, using the three lowest lattice momenta, $2\pi/L, 4\pi/L$ and $6\pi/L$. Larger momenta show a too bad signal-to-noise ratio in order to extract any meaningful result. We compute the real and the imaginary parts of the relevant matrix elements and find that the imaginary part is very important to give an asymmetry between the quark and anti-quark distributions, a highly non-trivial result of our calculation. In addition, we apply different levels of gauge link smearing in the operator. This smearing procedure has two effects. First, higher smearing levels reveal the asymmetry between quark and anti-quark distribution much clearer. Second, different smearing levels correspond to different renormalization properties of the matrix elements considered. Thus, comparing results from different smearing levels can give a hint about the importance of renormalization, depending on the size of effects from smearing. We will finally use the matching condition to relate the quasi-distribution to the real PDF and also apply nucleon target mass correction.

It needs to be stressed that the work presented here is only a very first step to understand the potential of the approach of Ref. [5]. It would be very important to look at larger momenta than used here to test that the perturbative matching works. Using a hypothetical mixed momentum setup (described below), we illustrate that a satisfactory agreement with phenomenological investigations could be obtained if larger momenta were available. We are planning to employ larger momenta in our next calculations by increasing our statistics by about an order of magnitude.

2 Theoretical setup

A method to calculate quark distributions directly on a Euclidean lattice has recently been proposed [5]. If successful, this method can greatly improve our comprehension of the structure of hadrons, as well as being the first *ab initio* QCD calculation of the Bjorken-x dependence of the quark distributions. The key observation in this proposal is that from the general form of the matrix element of a twist-2 operator between a nucleon state with momentum $P = (P_0, 0, 0, P_3)$,

$$\langle P|O^{\mu_1\mu_2\cdots\mu_n}|P\rangle = 2a_n^{(0)}\Pi^{\mu_1\mu_2\cdots\mu_n}, \tag{1}$$

a suitable choice of the indices $\mu_1, \mu_2, \ldots, \mu_n$ makes sure that the corresponding distribution is a purely spatial correlation. In Eq. (1), $a_n^{(0)}$ are the moments of the quark distributions and $\Pi^{\mu_1\mu_2\cdots\mu_n}$ is a symmetric rank - n tensor which can be formed with the target momentum P, as first calculated by Georgi and Politzer [20]. Let $n = 2k$, then

$$\Pi^{\mu_1\mu_2\cdots\mu_n} = \sum_{j=0}^{k}(-1)^j\frac{(2k-j)!}{2^j(2k)!}\{g...gP...P\}_{k,j}(P^2)^j, \tag{2}$$

where the term $\{g...gP...P\}_{k,j}$ means a symmetric sum of $(2k)!/2^j j!(2k-2j)!$ distinct products of the form $g^{\mu_1\mu_2}...g^{\mu_{2j-1}\mu_{2j}}P^{\mu_{2j+1}}...P^{\mu_{2k}}$. Thus, setting $\mu_1 = \mu_2 = ... = \mu_{2k} = 3$, one gets

$$\Pi^{3...3} = \sum_{j=0}^{k}(-1)^j\frac{(2k-j)!}{2^j(2k)!}\frac{(2k)!}{2^j j!(2k-2j)!}(-1)^j(P_3^2)^{k-j}(M^2)^j \tag{3}$$

or

$$\langle P|O^{3...3}|P\rangle = 2\tilde{a}_{2k}^{(0)}(P_3)^{2k}\sum_{j=0}^{k}\mu^j\begin{pmatrix} 2k-j \\ j \end{pmatrix} \equiv 2\tilde{a}_{2k}(P_3)^{2k}, \tag{4}$$

with $\mu = M^2/4(P_3)^2$ and M the nucleon mass. Here, we have introduced $\tilde{a}_{2k}$ as the matrix elements of the operator without subtracting the corrections in the nucleon mass. In the end, we want the matrix elements $\tilde{a}_{2k}^{(0)}$, which can be related to the usual moments of the quark distributions in the Infinite Momentum Frame (IMF). For now, we define

$$\tilde{a}_n(\Lambda, P_3) = \int_{-\infty}^{+\infty} x^{n-1}\tilde{q}(x, \Lambda, P_3)dx, \tag{5}$$

and apply the inverse Mellin transformation to Eq. (4) to obtain:

$$\tilde{q}(x, \Lambda, P_3) = \int_{-\infty}^{\infty}\frac{dz}{4\pi}e^{-izk_3}\langle P|\bar{\psi}(0,z)\gamma^3 W(z)\psi(0,0)|P\rangle, \tag{6}$$

where Λ is the UV regulator, $k_3 = xP_3$ is the quark momentum in the z-direction, and $W(z) = e^{-ig\int_0^z dz' A_3(z')}$ is the Wilson line introduced to make the quark distribution gauge invariant. Eq. (6) is called a quasi-distribution because it does not have the usual

properties of a quark distribution. Most notably, the momentum fraction x can be bigger than 1 or smaller than 0. Also, as discussed in Ref. [6], the calculation of the leading UV divergences to the quasi-distributions in perturbation theory are done keeping P_3 fixed while taking $\Lambda \to \infty$. This is in contrast to the case of the usual parton distributions, where one takes the limit $P_3 \to \infty$ first, that is, one first goes to the IMF. The dependence on the UV regulator, Λ, will be translated, in the end, into a renormalization scale μ when relating the quasi-distribution at finite P_3 to its counterpart at infinite P_3. For now, as we still do not have a renormalization procedure for the operator and the coupling, we freely identify the UV regulator in the perturbative corrections in the case of the IMF with μ, the renormalization scale, while keeping it as Λ for the case of the quasi-distributions.

To relate the quasi-distributions to the usual quark distributions, one uses the fact that the infrared region of the distributions is untouched when going from a finite to an infinite momentum. In other words, if $q(x,\mu)$ is the usual distribution defined though light-cone correlations, then one should have:

$$q(x,\mu) = q_{bare}(x)\left\{1 + \frac{\alpha_s}{2\pi} Z_F(\mu)\right\} + \frac{\alpha_s}{2\pi}\int_x^1 q^{(1)}(x/y,\mu) q_{bare}(y)\frac{dy}{y} + \mathcal{O}(\alpha_s^2), \qquad (7)$$

$$\tilde{q}(x,\Lambda,P_3) = q_{bare}(x)\left\{1 + \frac{\alpha_s}{2\pi} \tilde{Z}_F(\Lambda,P_3)\right\} + \frac{\alpha_s}{2\pi}\int_{x/x_c}^1 \tilde{q}^{(1)}(x/y,\Lambda,P_3) q_{bare}(y)\frac{dy}{y} + \mathcal{O}(\alpha_s^2), \qquad (8)$$

where q_{bare} is the bare distribution, Z_F and $\tilde{Z}_F$ are the wave function corrections and $q^{(1)}$ and $\tilde{q}^{(1)}$ are the vertex corrections. Notice that the lower limit of integration in Eq. (8) is x/x_c, where $x_c \sim \Lambda/P_3$ is the largest possible value of x which renders the vertex and wave function corrections to the quasi-distributions meaningful. Opposite to the infinite momentum calculation, at finite P_3 the terms $\tilde{Z}_F$ and $\tilde{q}^{(1)}$ do not vanish for $x > 1$, and thus this region has to be included, with the cut being made at $x > 1$, but below x_c. On the other hand, because $q^{(1)}(x,\mu) = 0$ for $x \geq 1$, the integration range in Eq. (7) can be extended down to x/x_c as well.

Lattice simulations can be used to calculate the left hand side of Eq. (8) through Eq. (6). Ideally, one would use perturbation theory to an arbitrary order to calculate the right hand side of Eqs. (7) and (8) to extract the quark distribution. Currently, however, the self-energy and vertex corrections are known to $\mathcal{O}(\alpha_s)$ only and for the non-singlet case [6]. With this in mind, Eqs. (7) and (8) can be combined to give

$$\begin{aligned}\tilde{q}(x,\Lambda,P_3) &= q(x,\mu) + \frac{\alpha_s}{2\pi} q(x,\mu)\left\{\tilde{Z}_F(\Lambda,P_3) - Z_F(\mu)\right\} \\ &\quad + \frac{\alpha_s}{2\pi}\int_{x/x_c}^1 \left(\tilde{q}^{(1)}(x/y,\Lambda,P_3) - q^{(1)}(x/y,\mu)\right) q(y,\mu)\frac{dy}{y} + \mathcal{O}(\alpha_s^2), \qquad (9)\end{aligned}$$

and this is equivalent to Eq. (13) of Ref. [6] if we consider quarks only. Notice that the quark number is conserved in the above expression, as long as the integrals $\tilde{Z}_F(\Lambda,P_3)$, listed in the Appendix, have also a cut in x_c. We define $\delta Z_F^{(1)}(\mu/P_3,\Lambda/P_3) = \tilde{Z}_F(\Lambda,P_3) - Z_F(\mu)$ and $Z^{(1)}(\xi,\mu/P_3,\Lambda/P_3) = \tilde{q}^{(1)}(\xi,\Lambda,P_3) - q^{(1)}(\xi,\mu)$. One can include antiquarks

using the crossing relation $\bar{q}(x) = -q(-x)$, and then rewrite Eq. (9) as

$$\begin{aligned} q(x,\mu) &= \tilde{q}(x,\Lambda,P_3) - \frac{\alpha_s}{2\pi}\tilde{q}(x,\Lambda,P_3)\delta Z_F^{(1)}\left(\frac{\mu}{P_3},\frac{\Lambda}{P_3}\right) \\ &\quad -\frac{\alpha_s}{2\pi}\int_{-1}^{1} Z^{(1)}\left(\frac{x}{y},\frac{\mu}{P_3},\frac{\Lambda}{P_3}\right)\tilde{q}(y,\Lambda,P_3)\frac{dy}{|y|} + \mathcal{O}(\alpha_s^2), \end{aligned} \tag{10}$$

where we have solved the system for $q(x,\mu)$. The form of Eq. (10) that we implement in the actual calculations is detailed in the Appendix.

Eq. (10) can be improved by calculating the corrections in M/P_3 to an arbitrary order. As before, we write $\tilde{a}_n^{(0)} = \int_{-\infty}^{+\infty} x^{n-1}\tilde{q}^{(0)}(x,P_z)dx$ and use this definition, together with Eq. (5), to Mellin invert Eq. (4). After some manipulation (*cf.* [21]), the result is:

$$\tilde{q}(x,P_z) = \frac{1}{1+\mu\xi^2}\tilde{q}^{(0)}(\xi,P_z), \tag{11}$$

where $\xi = \frac{2x}{1+\sqrt{1+4\mu x^2}}$ is the Nachtmann variable. The matching and the nucleon mass corrections are interchangeable.

3 Lattice calculation

In this section, we will describe our lattice setup and our lattice computations.

3.1 Matrix elements on the lattice

On the lattice, the bare matrix elements $h(P_3,z)$, which appear in Eq. (6), can be computed as

$$h(P_3,z) = \left\langle P|\overline{\psi}(z)\gamma_3 W_3(z,0)\psi(0)|P\right\rangle, \tag{12}$$

with the Euclidean momentum $P = (0,0,P_3,P_4)$ and $z = (0,0,z,0)$. Due to the (spatial) rotational symmetry on the lattice the computation can be straightforwardly applied to the other spatial directions. Our final result will then be an average over these three directions.

The required matrix elements can be obtained from the ratio of suitable two- and three-point functions. The three-point function is constructed with the use of nucleon interpolating fields and a local operator:

$$C^{3\mathrm{pt}}(t,\tau,0) = \left\langle N_\alpha(\vec{P},t)\mathcal{O}(\tau)\overline{N}_\alpha(\vec{P},0)\right\rangle, \tag{13}$$

where $\langle ...\rangle$ denotes the average over a sufficient number of gauge field configurations. A nucleon field boosted with a three-momentum can be defined via a Fourier transformation of quark fields in position space:

$$N_\alpha(\vec{P},t) = \Gamma_{\alpha\beta}\sum_{\vec{x}} \mathrm{e}^{i\vec{P}\vec{x}}\epsilon^{abc}u_\beta^a(x)\left(d^{bT}(x)\mathcal{C}\gamma_5 u^c(x)\right), \tag{14}$$

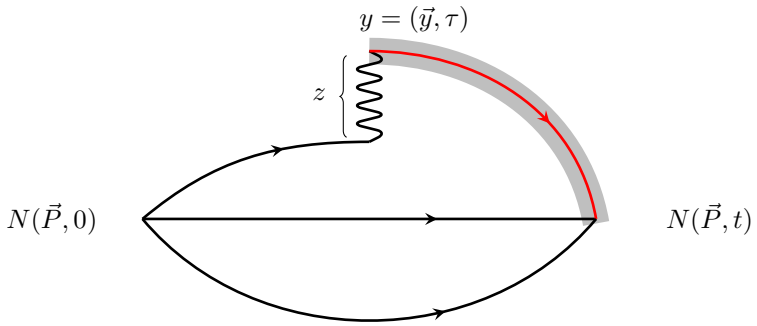

Figure 1: Schematic picture of a possible Wick contraction of the quark fields in the three-point function.

where $\mathcal{C} = i\gamma_0\gamma_2$ and $\Gamma_{\alpha\beta}$ is a suitable parity projector. Here, we will use the parity plus projector $\Gamma = \frac{1+\gamma_4}{2}$. The matrix element at vanishing momentum transfer ($Q^2 = 0$) can be obtained by choosing the following operator:

$$\mathcal{O}(z, \tau, Q^2 = 0) = \sum_{\vec{y}} \overline{\psi}(y + z)\gamma_3 W_3(y + z, y)\psi(y), \tag{15}$$

with $y = (\vec{y}, \tau)$. After Wick contracting the quark fields, the three-point function can be expressed in terms of quark propagators, see Fig. 1 for a schematic picture of such a contraction.

We can extract the matrix element from a ratio of the above given three- and two-point functions:

$$\frac{C^{3\text{pt}}(t, \tau, 0; \vec{P})}{C^{2\text{pt}}(t, 0; \vec{P})} \overset{0 \ll \tau \ll t}{=} \frac{-iP_3}{E} h(P_3, \Delta z), \tag{16}$$

where $E = \sqrt{(P_3)^2 + M^2}$ is the total energy of the nucleon and $C^{2\text{pt}}$ is the nucleon two-point function, which is constructed from the nucleon interpolating fields, $C^{2\text{pt}}(t, 0; \vec{P}) = \langle N_\alpha(\vec{P}, t)\overline{N}_\alpha(\vec{P}, 0)\rangle$. For the operator, we will consider the non-singlet, iso-vector quark combination, symbolically represented by $u-d$, which avoids disconnected contributions.

When computing the three-point function, there is a freedom on how to treat the propagator connecting the sink position with the operator insertion point (highlighted in Fig. 1). Due to momentum projection, there is a spatial sum on both ends of the propagator, which would naively require an all-to-all propagator. However, such a computation would need $V = L^3 \times T$ sets of inversions.

Here, we have tested two different methods to calculate the propagator. The first is the sequential method, which is exact. However, it requires the sink position and momentum to be fixed. As a second choice, we have used a stochastic method, where we use sources that contain Z^4 noise on one single time-slice (*cf.* Ref. [22]). The advantage of the stochastic method is its flexibility, allowing to freely choose the momentum at the sink position as well as vary the time-slide of the current insertion.

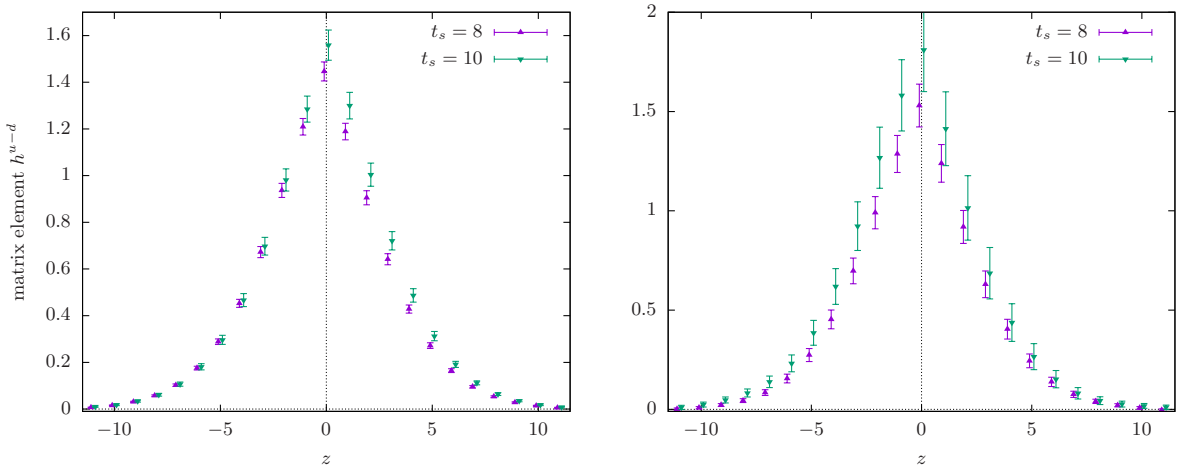

Figure 2: We show the results for the unrenormalized matrix elements for different source-sink separations t_s, **left**: $P_3 = 2\pi/L$, **right**: $P_3 = 4\pi/L$.

Results from an initial test on a smaller gauge ensemble [23] indicate that both methods show a compatible performance and give an approximately equal error for the same computational effort. Thus, for the following computations the stochastic method will be used, since it is more flexible for studying larger momenta.

3.2 Lattice setup

All results shown in this work are computed on a $32^3 \times 64$ lattice from an ETMC (European Twisted Mass Collaboration) production ensemble [24], with $N_f = 2 + 1 + 1$ flavors of maximally twisted mass fermions, *i.e.* two degenerate light quarks and non-degenerate strange and charm quarks. This ensemble has a bare coupling corresponding to $\beta = 1.95$, which yields a lattice spacing of $a \approx 0.082\,\text{fm}$ [11] and the twisted mass parameter $a\mu = 0.0055$, which corresponds to a pion mass of $m_{PS} \approx 370\,\text{MeV}$. Our present statistics to compute the matrix elements is 181 gauge configurations with 15 sets of forward and two sets of stochastic propagators, each set including both light (up and down) flavors, *i.e.* for 5430 measurements.

To examine the influence of excited states, the computation was done for two different source-sink separations: $8a$ and $10a$. From the comparison in Fig. 2, it can be seen that the results from both source-sink separations are visibly compatible within errors. It would require a significantly larger statistics to discriminate excited state effects, a task we want to address, however, in the future. Since here we perform an exploratory study, we will stick to the small separation of $8a$ due to the significantly smaller noise associated with it. This is especially advantageous for studying larger momenta, *e.g.* $P_3 = 6\pi/L$, which has generically a bad signal-to-noise ratio.

3.3 Lattice results

For our current statistics, we were able to extract matrix elements for $P_3 = 2\pi/L, 4\pi/L$ and $6\pi/L$. In Ref. [7], the authors applied HYP smearing [25] to the gauge links in the inserted operator, since this is expected to bring the necessary renormalization factors closer to the corresponding tree-level value. More generally speaking, such kind of smearing will certainly influence the renormalization properties of the considered matrix elements. In order to obtain an estimate how renormalization could influence the results which will be presented here, we applied two and five steps of HYP smearing to the operator and compare with the unsmeared results in Fig. 3.

Evidently, the effect of gauge link smearing changes the value of the matrix elements, for both the real and the imaginary parts. Note that the effect for the imaginary part is stronger than for the real part. Also, the change from zero to two steps of smearing is more significant than from two to five steps, which indicates a saturation of the smearing effect. We will therefore employ a maximum of five smearing steps in this work. We note in passing that a decrease of the noise like in other gluonic quantities, *e.g.* as in [26], cannot be observed when applying smearing. A striking observation in Fig. 3 is that while the real part is symmetric in z, the imaginary part is highly asymmetric. This effect will play an important role when we discuss the quark and anti-quark distributions later on.

Note that for a value of $z = 0$, the operator $\mathcal{O}$ in Eq. (15) can be identified with the local vector current at $Q^2 = 0$. This operator is renormalized with the vector current renormalization constant Z_V, which, for this ensemble, is $Z_V = 0.627(4)$ [27]. After renormalization, the condition $F_1^{u-d}(Q^2 = 0) = 1$ (*cf.* [28]) should hold. Indeed, we find $Z_V h^{u-d}(0) = 1.18(22)$ for $P_3 = 6\pi/L$ and $Z_V h^{u-d}(0) = 0.99(3)$ for $P_3 = 4\pi/L$ while the value for $P_3 = 2\pi/L$, $Z_V h^{u-d}(0) = 0.95(1)$, is a bit smaller, which is probably due to excited state effects[1]. For our final results, we will only use data obtained for $P_3 = 4\pi/L$ and $P_3 = 6\pi/L$.

As can be seen in Fig. 3, when going to larger values of P_3, the signal-to-noise ratio rapidly worsens. Thus, the calculation of a further, larger momentum is not possible with our present statistics.

4 Matching to quark distribution and nucleon mass corrections

From the matrix elements $h^{u-d}(z, P_3)$, we calculate the quasi-distributions and, after matching and nucleon mass corrections, the quark distributions themselves. To this end, we first apply the Fourier transformation to the nucleon matrix elements after multiplying by the vector current renormalization constant Z_V, using Eq. (6). From this equation, it is clear that if the imaginary part of the matrix elements were zero, or very close to zero, there would be no difference between the positive and negative x regions. In

[1] Using a larger source-sink separation of $10a$, we find $Z_V h^{u-d}(0) = 0.98(4)$, *cf.* Fig. 2, which is in agreement with one. We attribute the larger error to the larger source-sink separation and the fact that less measurements were used.

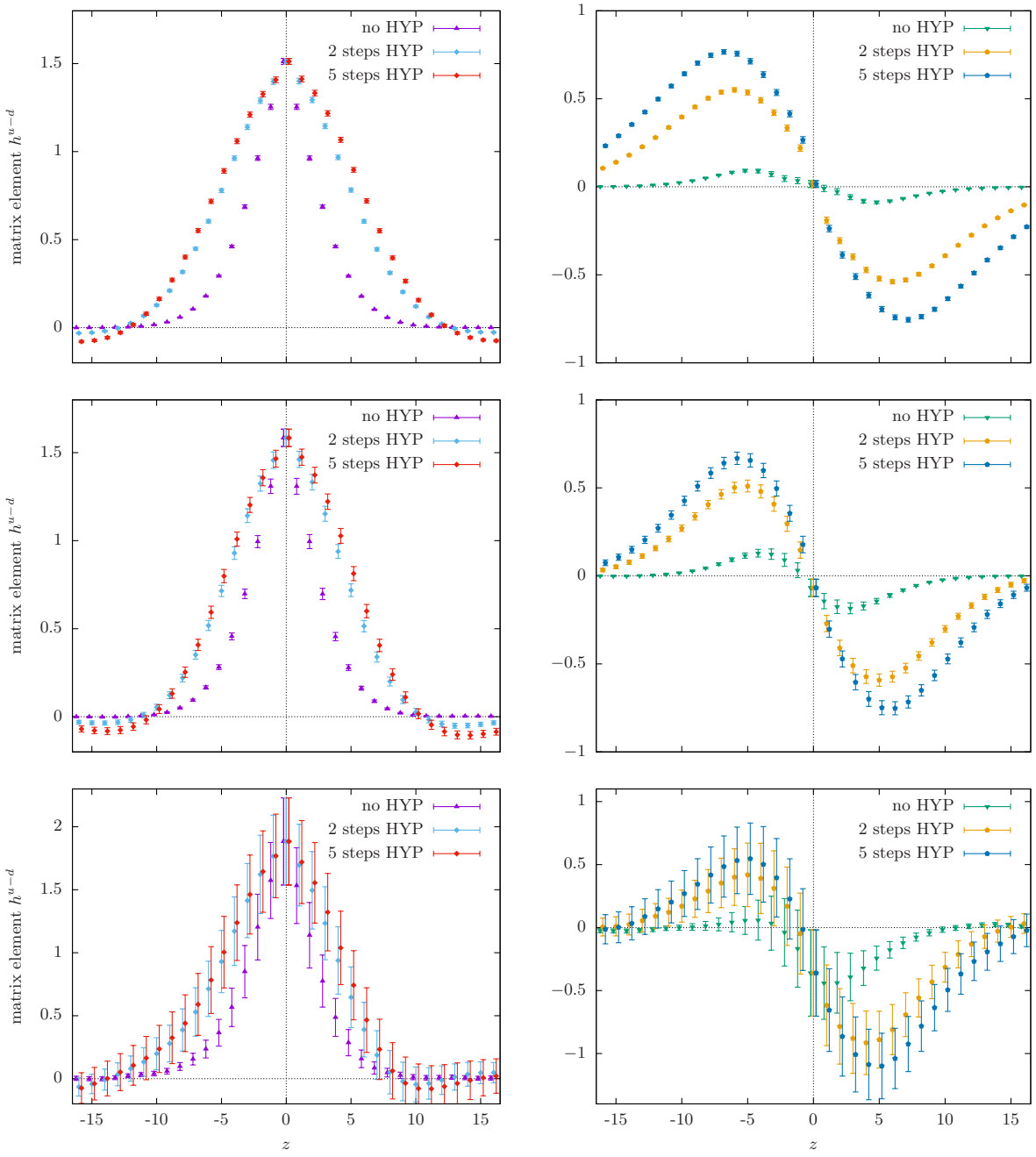

Figure 3: Results for the unrenormalized matrix elements with different steps of HYP smearing, **left**: real part, **right**: imaginary part, **from top to bottom**: $P_3 = 2\pi/L, 4\pi/L, 6\pi/L$.

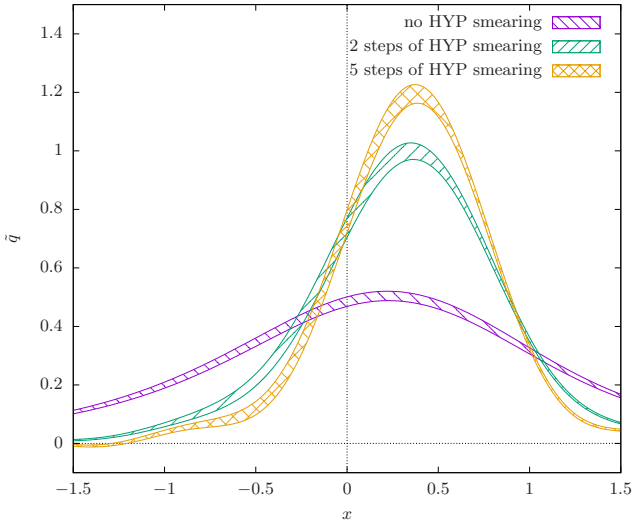

Figure 4: Comparison of results for $\tilde{q}$ obtained with five, two and no steps of HYP smearing, $P_3 = 4\pi/L$.

other words, there would be no difference between the quark and antiquark distributions, as antiquarks can be interpreted as quarks in the negative x region, according to the crossing relation $\overline{q}(x) = -q(-x)$.

Fig. 4 shows the complete quasi-distribution for $P_3 = 4\pi/L$, after applying the Fourier transformation and taking the real and the imaginary parts of $h^{u-d}(z, P_3)$ into account. An asymmetry between negative and positive x values is clearly building up, which is more pronounced for higher levels of gauge link smearing, emphasizing the effect of HYP smearing on the renormalization of these quantities Because after a proper renormalization the results with non-smeared and smeared gauge links have to agree within errors, the effect seen in Fig. 4 clearly points to the fact that renormalization will play an important role when looking at the quark distributions obtained from lattice calculations in the future.

Having the quasi-distribution $\tilde{q}(x)$, we can proceed to extract the physical quark distribution $q(x)$ from $\tilde{q}(x)$, using Eq. (24) and then applying the nucleon mass corrections. To be consistent, the value of the momentum cutoff is chosen to be the same as the value of the lattice cutoff itself, that is, $\Lambda = 1/a \cong 2.5\,\text{GeV}$. For the renormalization scale μ we make the same choice. This is a somewhat *ad hoc*, but plausible choice. Once a proper renormalization has been carried out, the full equations for the running with μ will be obtained.

As discussed in the Appendix, the integrals also have a cut-off at $x_c \sim \Lambda/P_3$, such that $\tilde{q}(x > x_c, \Lambda, P_3) = 0$. The last input we need for our calculation is the bare coupling constant, for which we use the value corresponding to $\beta = 1.95$ of our lattice calculation. This leads to $\alpha_s = 6/(4\pi\beta) \approx 0.245$.

We show our results in Fig. 5 for the case of 0, 2, and 5 steps of HYP smearing, for a nucleon with momentum $P_3 = 4\pi/L$ and $P_3 = 6\pi/L$, corresponding to 0.98 GeV and 1.47 GeV, respectively. As anticipated, HYP smearing is essential in providing the

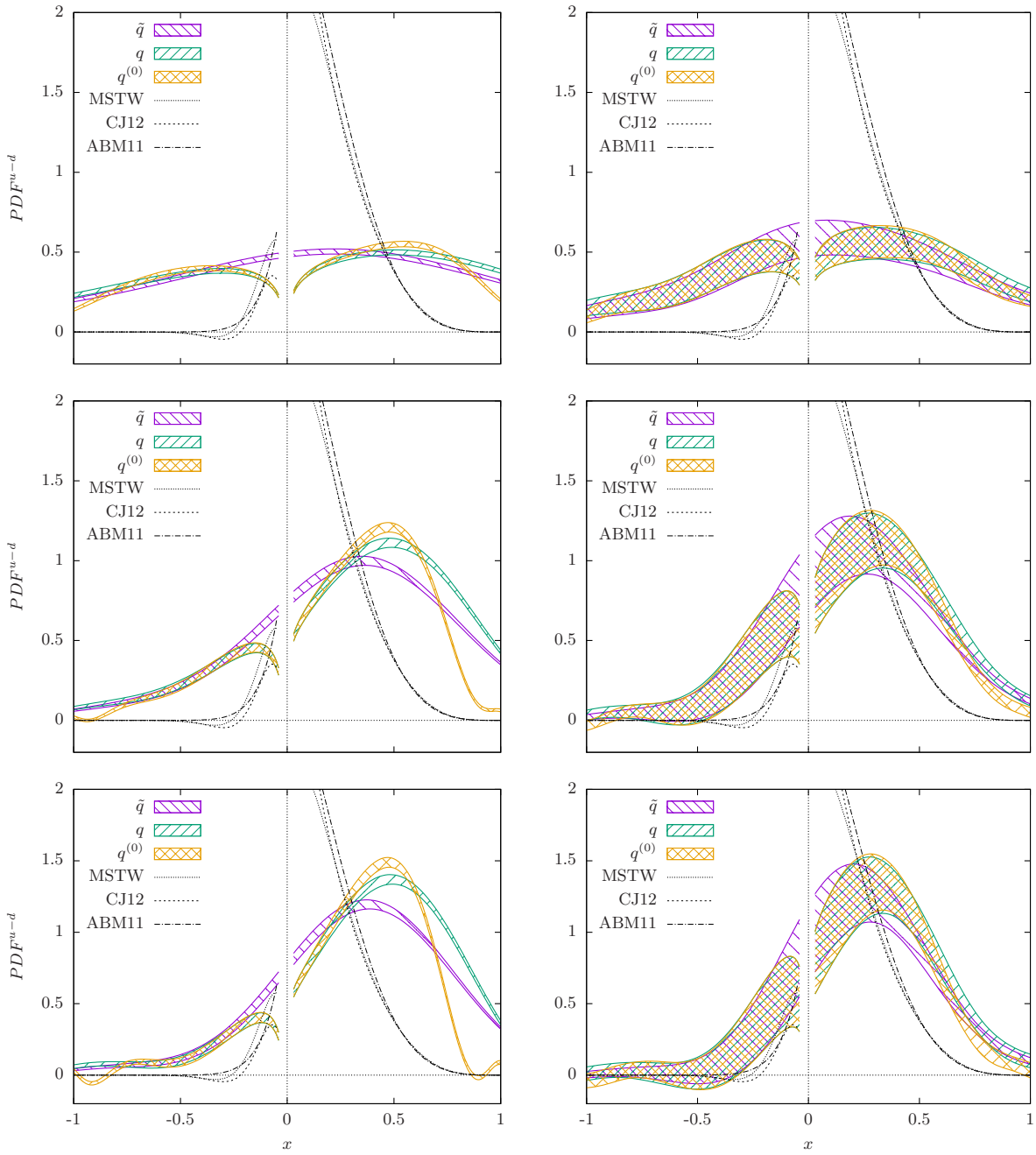

Figure 5: The resulting quasi-distribution $\tilde{q}$, PDF without subtracting the mass correction q, and final PDF $q^{(0)}$, **left**: $P_3 = 4\pi/L$, **right**: $P_3 = 6\pi/L$, **from top to bottom**: 0 steps, 2 steps, 5 steps of HYP smearing, negative region: $\bar{q}(x) = -q(-x)$, comparison with phenomenological $u(x) - d(x)$ curves at $Q^2 = 6.25\,\mathrm{MeV}^2$ (MSTW [29], CJ12 [30], ABM11 [31]).

required asymmetry between the quark and antiquark distributions. We note that two steps of smearing are already practically sufficient to show the effect of the asymmetry.

As the nucleon momentum increases, the peak of the $u(x) - d(x)$ distribution moves to smaller values of x, as it should, while for $\overline{d}(x) - \overline{u}(x)$ it gets closer to 0 for most of the x region, but shows an increase in the small x region. This behavior is in qualitative agreement with the behavior of the antiquark distributions as extracted from phenomenological analyses [29, 30, 31]. The nucleon mass corrections lead to a decrease of the distributions in the large x region. This is again in full accordance with our expectation from phenomenology and asserts that the nucleon mass corrections are essential to restore the energy-momentum relations, thus ensuring the partonic interpretation of the distributions. In addition, with increasing nucleon momentum the mass corrections become less and less important, as expected from Eq. (11). Finally, the slight oscillatory behavior in the large x region is a result of performing the Fourier transformation over a finite extension only, in our case the integration is from $-L/2$ to $+L/2$. Because the nucleon mass corrections also make a shift of the distributions from larger to smaller values of x, the oscillatory behavior is more pronounced after Eq. (11) is applied, as the oscillations are more noticeable in the quasi-distributions in the region $x > 1$. Increasing the value of P_3 is similar to extending the bounds of integration and thus reduces the oscillations. On this same line, if we had used ± 1 as the limits of of integration in the matching, as in Eq. (10) and thus not taking into account the $x > \xi$ region in the last two terms of Eq. (24), the oscillations would be slightly more pronounced for the case of $P_3 = 4\pi/L$. For $P_3 = 6\pi/L$ there would be no real difference to the results presented in Fig. 5.

Although we find that the shape of the quark distributions resembles those of the phenomenological parametrizations of $u(x) - d(x)$, with 2 or 5 steps of HYP smearing, we do not find an agreement on the quantitative level. Note, however, that there is a clear tendency to approach the phenomenological parametrizations when P_3 is increased. Motivated by this observation, we made an exploratory study where we use the matrix elements calculated with $P_3 = 4\pi/L$ and $P_3 = 6\pi/L$, but perform the Fourier transformation in Eq. (6), as well as the matching and the nucleon mass corrections, with $P_3 = 8\pi/L$. We will refer to this particular setup as the mixed momentum setup. The resulting distributions are shown in Fig. 6.

It needs to be stressed that this exercise is, of course, only hypothetical. Nevertheless, the agreement with the phenomenological parametrizations of the distributions at the intermediate and large x regions is really encouraging. This indicates that by employing an only moderately larger value of P_3 than the ones used here, we could obtain even a quantitative agreement to the parametrizations in certain regions of x. This concerns in particular the large x region, where increasing values of P_3 tend to bring the resulting distribution down. In the small (and positive) x region, on the other hand, it seems that increasing the nucleon momentum is not sufficient to produce a rise of the distribution. This may be related to the fact that there is a limitation in the present calculation in the small x region due to the presence of the infrared, $1/L$, and ultra-violet, $1/a$ cut-off regulators on a finite lattice. Thus, this limitation will be overcome when larger lattices and smaller values of the lattice spacing become available. In any case, a more

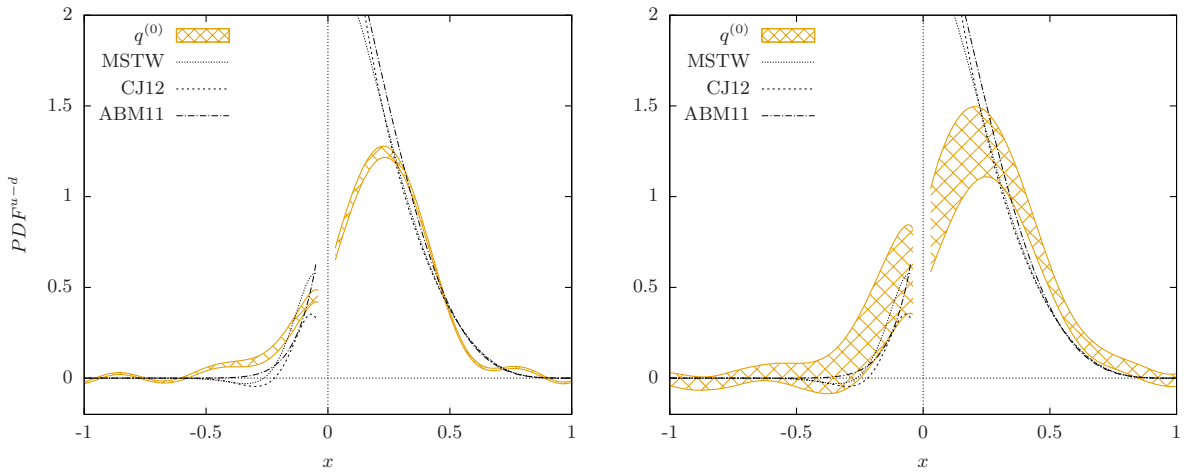

Figure 6: Results from an analysis using different values of the momentum in the computation of the lattice matrix element (**left**: $P_3 = 4\pi/L$, **right**: $P_3 = 6\pi/L$) than in the matching and mass corrections ($P_3 = 8\pi/L$) with 5 steps of HYP smearing.

definite statement can only be made after we have access to the matrix elements for $P_3 = 8\pi/L$. This is not possible with our present statistics. However, we are in the process of generating a substantially higher statistics. This will allow us to extrapolate the data for $P_3 = 2\pi/L$, $P_3 = 4\pi/L$ and $P_3 = 6\pi/L$ to obtain the quasi-distribution at $P_3 = 8\pi/L$. Although we do not expect a big difference to the situation of the hypothetical mixed setup shown in Fig. 6, a full analysis with real data is, of course, mandatory and will be presented in a forthcoming work.

5 Conclusions and outlook

In this work, we have presented our first exploratory study of the approach developed in Ref. [5] for the calculation of the x dependence of quark distributions directly on the lattice, employing the twisted mass formulation of lattice QCD. The study presented here, together with the work of Ref. [7], constitute the first two attempts to implement the approach of Ref. [5] in realistic lattice QCD calculations. Our results, represented in Fig. 5, are comparable to those of Fig. 2 of [7] and we see that the two calculations give similar results for the case of 2 steps of HYP smearing. Yet it seems that in our case, for $P_3 = 6\pi/L$, the shift of the peak of the quark distributions towards the small x region is bigger. Also, as we increase the number of steps of HYP smearing, the position of the peaks is basically unchanged, but they are more pronounced. On the other hand, the large x region tends to be smaller. It is very reassuring to see that both effects bring our results closer to the phenomenological parametrizations. Beyond these effects, HYP smearing is fundamental to generate a sizeable (asymmetric in z) imaginary part in the matrix elements. This result generates automatically an asymmetry between the quark and the antiquark distributions, a highly non-trivial result.

The outcome of our *ab initio* lattice QCD calculation with a small and positive

$\overline{d}(x) - \overline{u}(x)$ is in a very good qualitative agreement with phenomenological parametrizations. In a hypothetical exercise where we use a larger momentum of $P_3 = 8\pi/L$ in the Fourier transformation than we actually have in our lattice QCD calculation, we observe a better qualitative behavior as compared to what is expected phenomenologically, as is shown in Fig. 6. Moreover, it is clear from both Figs. 5 and 6 that increasing the momentum implies only marginal corrections to the quasi-distributions, the corrections for the case $P_3 = 6\pi/L$ being restricted from intermediate to small x regions only.

In summary, we have presented our first effort to explore the potential to calculate quark distributions directly within the lattice QCD formulation. Although there are clearly shortcomings, such as not being able to reach large momenta and the lack of renormalization, our results are promising. In particular, our study of the quark distribution in the mixed momentum setup indicates that only moderately larger momenta than used here may be sufficient to reach a quantitative agreement with phenomenological parametrizations in the large x region. We are presently increasing our statistics significantly, which will allow us to obtain data with such larger momenta. In addition, we are testing different approaches to perform the necessary renormalization of the matrix elements entering the calculation of the quasi-distributions. Finally, applying this method to gluon configurations generated directly at the physical value of the pion mass may open the exciting possibility to address quark distributions and therefore unravel the structure of hadron from first principle QCD calculations.

Acknowledgments

We thank our fellow members of ETMC for their constant collaboration. In particular helpful discussions with G.C. Rossi are gratefully acknowledged.

We are grateful to the John von Neumann Institute for Computing (NIC), the Jülich Supercomputing Center and the DESY Zeuthen Computing Center for their computing resources and support.

This work has been supported in part by the DFG Sonderforschungsbereich/Transregio SFB/TR9 and by the Cyprus Research Promotion Foundation through the Project Cy-Tera (NEA ΥΠΟΔΟΜΗ/ΣΤΡΑΤΗ/0308/31) co-financed by the European Regional Development Fund. VD was supported by the Danish National Research Foundation DNRF:90 grant and by a Lundbeck Foundation Fellowship grant. FS was supported by CNPq contract number 249168/2013-8.

Appendix

The wave function and vertex corrections in Eq. (10) were calculated in Ref. [6]. The vertex corrections are given by:

$$\frac{Z^{(1)}(\xi)}{C_F} = \left(\frac{1+\xi^2}{1-\xi}\right)\ln\frac{\xi}{\xi-1} + 1 + \frac{1}{(1-\xi)^2}\frac{\Lambda}{P_3} \tag{17}$$

for $\xi > 1$,

$$\frac{Z^{(1)}(\xi)}{C_F} = \left(\frac{1+\xi^2}{1-\xi}\right)\ln\frac{(P_3)^2}{\mu^2} + \left(\frac{1+\xi^2}{1-\xi}\right)\ln 4\xi(1-\xi) - \frac{2\xi}{1-\xi} + 1 + \frac{1}{(1-\xi)^2}\frac{\Lambda}{P_3} \tag{18}$$

for $0 < \xi < 1$,

$$\frac{Z^{(1)}(\xi)}{C_F} = \left(\frac{1+\xi^2}{1-\xi}\right)\ln\frac{\xi-1}{\xi} - 1 + \frac{1}{(1-\xi)^2}\frac{\Lambda}{P_3} \tag{19}$$

for $\xi < 0$. The wave function corrections are given by:

$$\delta Z^{(1)} = C_F \int_{-\infty}^{\infty} d\xi\, \delta Z^{(1)}(\xi), \tag{20}$$

where

$$\delta Z^{(1)}(\xi) = -\left(\frac{1+\xi^2}{1-\xi}\right)\ln\frac{\xi}{\xi-1} - 1 - \frac{1}{(1-\xi)^2}\frac{\Lambda}{P_3} \tag{21}$$

for $\xi > 1$,

$$\delta Z^{(1)}(\xi) = -\left(\frac{1+\xi^2}{1-\xi}\right)\ln\frac{(P_3)^2}{\mu^2} - \left(\frac{1+\xi^2}{1-\xi}\right)\ln 4\xi(1-\xi) - \frac{2\xi(2\xi-1)}{1-\xi} + 1 - \frac{1}{(1-\xi)^2}\frac{\Lambda}{P_3} \tag{22}$$

for $0 < \xi < 1$,

$$\delta Z^{(1)}(\xi) = -\left(\frac{1+\xi^2}{1-\xi}\right)\ln\frac{\xi-1}{\xi} + 1 - \frac{1}{(1-\xi)^2}\frac{\Lambda}{P_3} \tag{23}$$

for $\xi < 0$.

In the actual calculation, we make a change of variables in the integral term containing $\tilde{q}(y, \Lambda, P_3)$ of Eq. (10), and also set the threshold above which the quasi-distribution is zero. We call this value x_c, which is of order of Λ/P_3. When we inverted Eq. (9), we kept the limits of integration from -1 to +1, which is the region where the quark distributions are defined and where factorization holds. In practice, we will integrate from $-x_c$ to $+x_c$, the reason being that $\tilde{q}(x > 1) \neq 0$ and contributions from this region should be taken into account. As we increase the value of P_3, however, the closer we get to the physical distribution and as a result $\tilde{q}(x > 1) \sim 0$. We also break the integral containing $\tilde{q}$ into two terms, with the limits from $-x_c$ to $-|x|/x_c$ and from $+|x|/x_c$ to $+x_c$. We then make a change of variables, $\xi = x/y$, and Eq. (10) is rewritten as:

$$
\begin{aligned}
q(x,\mu) &= \tilde{q}(x,\Lambda,P_3) - \frac{\alpha_s}{2\pi}\tilde{q}(x,\Lambda,P_3)\delta Z^{(1)}\left(\frac{\mu}{P_3},\frac{\Lambda}{P_3}\right) \\
&\quad -\frac{\alpha_s}{2\pi}\int_{-x_c}^{-|x|/x_c} Z^{(1)}\left(\xi,\frac{\mu}{P_3},\frac{\Lambda}{P_3}\right)\tilde{q}\left(\frac{x}{\xi},\Lambda,P_3\right)\frac{d\xi}{|\xi|} \\
&\quad -\frac{\alpha_s}{2\pi}\int_{+|x|/x_c}^{+x_c} Z^{(1)}\left(\xi,\frac{\mu}{P_3},\frac{\Lambda}{P_3}\right)\tilde{q}\left(\frac{x}{\xi},\Lambda,P_3\right)\frac{d\xi}{|\xi|} + \mathcal{O}(\alpha_s^2). \qquad (24)
\end{aligned}
$$

The integrals contain both single and double poles at $\xi = 1$. It can be shown that he single pole terms cancel between Eqs. (17)-(18) and (21)-(22), *e.g.* the single pole in the third term on the l.h.s of Eq. (18) is cancelled by the third term on the l.h.s of Eq. (22). The double poles are first reduced to a single pole by a similar cancellation when combining the vertex and wave function corrections, as in the single pole case, and the remaining pole is taken care of by using the Cauchy's principal value prescription. The remaining expression is finite, with the exception that the integral of $\delta Z^{(1)}(\xi)$ is divergent as $\xi \to \pm\infty$. The divergent term is:

$$
\tilde{q}(x)\frac{3}{2}\ln(x_c^2 - 1), \qquad (25)
$$

where we have set x_c as the upper and lower limit of the integrals of (21) and (23), respectively. The same limits of integration, both when integrating $Z^{(1)}$ and $\delta Z^{(1)}$ are necessary in order to maintain the quark number conservation. Notice that this log divergent term is the usual UV divergence present in the wave function.

References

[1] C. Alexandrou, M. Constantinou, V. Drach, K. Hatziyiannakou, K. Jansen, *et al.*, "Nucleon Structure using lattice QCD," *Nuovo Cim.* **C036** no. 05, (2013) 111–120, arXiv:1303.6818 [hep-lat].

[2] C. Alexandrou, "Nucleon structure from lattice QCD - recent achievements and perspectives," *EPJ Web Conf.* **73** (2014) 01013, arXiv:1404.5213 [hep-lat].

[3] S. Syritsyn, "Review of Hadron Structure Calculations on a Lattice," *PoS* **LATTICE2013** (2014) 009, arXiv:1403.4686 [hep-lat].

[4] M. Constantinou, "Hadron Structure," *PoS* **LATTICE2014** (2014) 001, arXiv:1411.0078 [hep-lat].

[5] X. Ji, "Parton Physics on a Euclidean Lattice," *Phys.Rev.Lett.* **110** (2013) 262002, arXiv:1305.1539 [hep-ph].

[6] X. Xiong, X. Ji, J.-H. Zhang, and Y. Zhao, "One-loop matching for parton distributions: Nonsinglet case," *Phys.Rev.* **D90** no. 1, (2014) 014051, arXiv:1310.7471 [hep-ph].

[7] H.-W. Lin, J.-W. Chen, S. D. Cohen, and X. Ji, "Flavor Structure of the Nucleon Sea from Lattice QCD," *Phys.Rev.* **D91** (2015) 054510, arXiv:1402.1462 [hep-ph].

[8] R. Frezzotti and G. Rossi, "Chirally improving Wilson fermions. 1. O(a) improvement," *JHEP* **0408** (2004) 007, arXiv:hep-lat/0306014 [hep-lat].

[9] **European Twisted Mass Collaboration** Collaboration, C. Alexandrou *et al.*, "Light baryon masses with dynamical twisted mass fermions," *Phys.Rev.* **D78** (2008) 014509, arXiv:0803.3190 [hep-lat].

[10] **ETM Collaboration** Collaboration, C. Alexandrou *et al.*, "Low-lying baryon spectrum with two dynamical twisted mass fermions," *Phys.Rev.* **D80** (2009) 114503, arXiv:0910.2419 [hep-lat].

[11] C. Alexandrou, V. Drach, K. Jansen, C. Kallidonis, and G. Koutsou, "Baryon spectrum with $N_f = 2 + 1 + 1$ twisted mass fermions," *Phys.Rev.* **D90** no. 7, (2014) 074501, arXiv:1406.4310 [hep-lat].

[12] **ETM Collaboration** Collaboration, C. Alexandrou *et al.*, "Axial Nucleon form factors from lattice QCD," *Phys.Rev.* **D83** (2011) 045010, arXiv:1012.0857 [hep-lat].

[13] C. Alexandrou, J. Carbonell, M. Constantinou, P. Harraud, P. Guichon, *et al.*, "Moments of nucleon generalized parton distributions from lattice QCD," *Phys.Rev.* **D83** (2011) 114513, arXiv:1104.1600 [hep-lat].

[14] C. Alexandrou, M. Brinet, J. Carbonell, M. Constantinou, P. Harraud, *et al.*, "Nucleon electromagnetic form factors in twisted mass lattice QCD," *Phys.Rev.* **D83** (2011) 094502, arXiv:1102.2208 [hep-lat].

[15] S. Dinter, C. Alexandrou, M. Constantinou, V. Drach, K. Jansen, *et al.*, "Precision Study of Excited State Effects in Nucleon Matrix Elements," *Phys.Lett.* **B704** (2011) 89–93, arXiv:1108.1076 [hep-lat].

[16] C. Alexandrou, M. Constantinou, S. Dinter, V. Drach, K. Jansen, *et al.*, "Nucleon form factors and moments of generalized parton distributions using $N_f = 2 + 1 + 1$ twisted mass fermions," *Phys.Rev.* **D88** no. 1, (2013) 014509, arXiv:1303.5979 [hep-lat].

[17] C. Alexandrou, K. Hadjiyiannakou, G. Koutsou, A. O'Cais, and A. Strelchenko, "Evaluation of fermion loops applied to the calculation of the η' mass and the nucleon scalar and electromagnetic form factors," *Comput.Phys.Commun.* **183** (2012) 1215–1224, arXiv:1108.2473 [hep-lat].

[18] A. Abdel-Rehim, C. Alexandrou, M. Constantinou, V. Drach, K. Hadjiyiannakou, *et al.*, "Disconnected quark loop contributions to nucleon observables in lattice QCD," *Phys.Rev.* **D89** no. 3, (2014) 034501, arXiv:1310.6339 [hep-lat].

[19] C. Alexandrou, M. Constantinou, V. Drach, K. Hadjiyiannakou, K. Jansen, *et al.*, "Evaluation of disconnected quark loops for hadron structure using GPUs," *Comput.Phys.Commun.* **185** (2014) 1370–1382, arXiv:1309.2256 [hep-lat].

[20] H. Georgi and H. D. Politzer, "Freedom at Moderate Energies: Masses in Color Dynamics," *Phys.Rev.* **D14** (1976) 1829.

[21] F. Steffens, M. Brown, W. Melnitchouk, and S. Sanches, "Parton distributions in the presence of target mass corrections," *Phys.Rev.* **C86** (2012) 065208, arXiv:1210.4398 [hep-ph].

[22] **ETM** Collaboration, C. Alexandrou *et al.*, "A Stochastic Method for Computing Hadronic Matrix Elements," *Eur.Phys.J.* **C74** no. 1, (2014) 2692, arXiv:1302.2608 [hep-lat].

[23] C. Alexandrou, K. Cichy, V. Drach, E. Garcia-Ramos, K. Hadjiyiannakou, *et al.*, "First results with twisted mass fermions towards the computation of parton distribution functions on the lattice," *PoS* **LATTICE2014** (2014) 135, arXiv:1411.0891 [hep-lat].

[24] R. Baron, P. Boucaud, J. Carbonell, A. Deuzeman, V. Drach, *et al.*, "Light hadrons from lattice QCD with light (u,d), strange and charm dynamical quarks," *JHEP* **1006** (2010) 111, arXiv:1004.5284 [hep-lat].

[25] A. Hasenfratz and F. Knechtli, "Flavor symmetry and the static potential with hypercubic blocking," *Phys.Rev.* **D64** (2001) 034504, arXiv:hep-lat/0103029 [hep-lat].

[26] C. Alexandrou, V. Drach, K. Hadjiyiannakou, K. Jansen, B. Kostrzewa, *et al.*, "Looking at the gluon moment of the nucleon with dynamical twisted mass fermions," *PoS* **LATTICE2013** (2014) 289, arXiv:1311.3174 [hep-lat].

[27] C. Alexandrou, M. Constantinou, T. Korzec, H. Panagopoulos, and F. Stylianou, "Renormalization constants of local operators for Wilson type improved fermions," *Phys.Rev.* **D86** (2012) 014505, arXiv:1201.5025 [hep-lat].

[28] P. Hagler, "Hadron structure from lattice quantum chromodynamics," *Phys.Rept.* **490** (2010) 49–175, arXiv:0912.5483 [hep-lat].

[29] A. Martin, W. Stirling, R. Thorne, and G. Watt, "Parton distributions for the LHC," *Eur.Phys.J.* **C63** (2009) 189–285, arXiv:0901.0002 [hep-ph].

[30] J. Owens, A. Accardi, and W. Melnitchouk, "Global parton distributions with nuclear and finite-Q^2 corrections," *Phys.Rev.* **D87** no. 9, (2013) 094012, arXiv:1212.1702 [hep-ph].

[31] S. Alekhin, J. Blumlein, and S. Moch, "Parton Distribution Functions and Benchmark Cross Sections at NNLO," *Phys.Rev.* **D86** (2012) 054009, arXiv:1202.2281 [hep-ph].